Development of Novel PSMA Ligands for Imaging and Therapy with Copper Isotopes

José Carlos dos Santos[1], Barbro Beijer[1], Ulrike Bauder-Wüst[2], Martin Schäfer [2], Karin Leotta[1], Matthias Eder[3], Martina Benešová[2], Christian Kleist[1], Frederik Giesel[1], Clemens Kratochwil[1], Klaus Kopka[2], Uwe Haberkorn[1,4], and Walter Mier[1]

[1]Department of Nuclear Medicine, Heidelberg University Hospital, Heidelberg, Germany; [2]Division of Radiopharmaceutical Chemistry, German Cancer Research Center, Heidelberg, Germany; [3]Division of Radiopharmaceutical Development, German Cancer Consortium Freiburg, Department of Nuclear Medicine, University of Freiburg, Freiburg, Germany; and [4]Clinical Cooperation Unit Nuclear Medicine, German Cancer Research Center, Heidelberg, Germany

Prostate-specific membrane antigen (PSMA)–binding tracers have been shown to be promising agents for the specific targeting of prostate tumors. On labeling with the short-lived isotopes ^{18}F and ^{68}Ga, excellent molecular imaging performance is achieved. This potential could be further exploited using long-lived isotopes. Because of the favorable half-life of ^{64}Cu, tracers labeled with this PET nuclide could solve logistic problems. Moreover, this isotope provides a theranostic pair with the therapeutic copper isotope ^{67}Cu. Hence, 9 novel tracers that combine dedicated copper chelators with the PSMA-specific urea-based binding motif were developed. **Methods:** The precursors were obtained by solid-phase synthesis. The purity and molecular weight of the PSMA ligands were confirmed by high-performance liquid chromatography and liquid chromatography–mass spectrometry. The compounds were labeled with ^{64}Cu, with a radiolabeling yield of more than 99%. Competitive cell binding assays and internalization assays were performed with C4-2 cells, a subline of the PSMA-positive cell line LNCaP (human lymph node carcinoma of the prostate). In vitro serum stability, the stability of ^{64}Cu-CA003 in blood, and the in vivo fate of neat ^{64}Cu-chloride or ^{64}Cu-CA003 were determined to prove whether the stability of the radiolabeled compounds is sufficient to ensure no significant loss of copper during the targeting process. For PET imaging and biodistribution studies, a C4-2 tumor–bearing mouse model was used. **Results:** The radiolabeled ^{64}Cu-PSMA ligands showed high serum stability. All PSMA ligands showed high inhibition potencies, with equilibrium inhibition constants in the low nanomolar range. ^{64}Cu-CA003 and ^{64}Cu-CA005 showed high internalization ratios (34.6% ± 2.8 and 18.6% ± 4.4, respectively). Both the in vitro serum stability determination and the in vivo characterization of the main radiolabeled compounds confirmed that, except for ^{64}Cu-PSMA-617, all compounds showed high serum stability within the observation period of 24 h. Small-animal PET imaging demonstrated high tumor uptake within 20 min. Organ distribution studies confirmed high specific uptake in the tumor, with 30.8 ± 12.6 percentage injected dose (%ID)/g at 1 h after injection. Rapid clearance from the kidneys was observed—a decrease from 67.0 ± 20.9 %ID/g at 1 h after injection to 7.5 ± 8.51 %ID/g at 24 h after injection (in the case of CA003). The performance of CA003, the compound with the best preclinical properties, was assessed in a first patient. In line with its preclinical data, PET imaging resulted in clear visualization of the cancer lesions, with high contrast. **Conclusion:** The ^{64}Cu-labeled PSMA ligands are promising agents to target PSMA and visualize PSMA-positive tumor lesions as shown in preclinical evaluation by small-animal PET studies, organ distribution, and a patient application. Most importantly, the images obtained at 20 h enabled delineation of unclear lesions, showing that the compounds fulfill the prerequisite for dosimetry in the course of therapy planning with ^{67}Cu. Thus, we suggest clinical use of copper-labeled CA003 for diagnostics and radiotherapy of prostate cancer.

Key Words: PSMA; copper radioisotopes; radiotracer; prostate cancer; PET imaging; endoradiotherapy

J Nucl Med 2020; 61:70–79
DOI: 10.2967/jnumed.119.229054

Prostate-specific membrane antigen (PSMA) is overexpressed in most cases of prostate cancer, and its expression level correlates with progression of the disease. Furthermore, expression increases during the metastatic process (*1–3*). In the last few years, several PSMA ligands, including antibodies such as ^{111}In-capromab pendetide and ^{111}In-HuJ591, have proven promising for targeting, as well as for molecular imaging of prostate tumors (*4–9*). Radiotracers with excellent tumor-to-background ratios and high overall tumoral uptake were developed, and a variety of small-molecule imaging agents for prostate cancer is being pursued clinically. Among them, the following can be highlighted: ^{11}C-choline (*10*); ^{18}F-choline (*11*); ^{18}F-DCFPyl (*12*); ^{18}F-DCFBC (*13*); ^{68}Ga-, ^{111}In-, and ^{177}Lu-PSMA I&T (*14*);^{124}I/^{131}I-labeled MIP-1095 (*15*); ^{99m}Tc-MIP-1404 (*16*); ^{68}Ga-PSMA-11 (*5*); ^{68}Ga-, ^{177}Lu-, ^{213}Bi-, and ^{225}Ac-PSMA-617 (*6,17*); ^{18}F-PSMA-1007 (*7*); and PSMA-7 (*18*). ^{68}Ga-PSMA-11 is one of the most relevant radiotracers and currently in clinical use to detect prostate cancer. Studies of PSMA-11 in patients demonstrated high tumor uptake already at 1 h after injection, and because of its specificity, images of high contrast are obtained (*19*). Recently, a new Glu-urea-Lys-$(HE)_3$-HBED-CC analog of PSMA-11 revealed lower spleen and kidney uptake and was shown to be a promising tracer for clinical PET/CT (*20*). One limitation of the chelator HBED-CC is that it does not allow the formation of stable chelate complexes with the most relevant therapeutic radionuclides.

Because of the high demand for therapeutic radiotracers, PSMA-617 was developed. It can be labeled with many relevant therapeutic

Received Mar. 22, 2019; revision accepted Jun. 12, 2019.
For correspondence or reprints contact: Walter Mier, Department of Nuclear Medicine, Heidelberg University Hospital, Im Neuenheimer Feld 400, 69120 Heidelberg, Germany.
E-mail: walter.mier@med.uni-heidelberg.de
Published online Sep. 20, 2019.

radionuclides, such as ^{90}Y, ^{177}Lu, ^{213}Bi, and ^{225}Ac. When labeled with ^{68}Ga, this radiotracer can be used for diagnostic purposes (*6,17,21*).

The Lys-NH-CO-NH-Glu moiety had been shown to target PSMA with high affinity. PSMA-11 and PSMA-617 contain this binding motif (*22,23*). In the case of PSMA-617, the 2 linker moieties 2-naphthyl-L-alanine and 4-(aminomethyl)cyclohexanecarboxylic acid were shown to be successful (Fig. 1). These components optimize the pharmacokinetic properties, leading to a high internalization ratio and consequently high PET image contrast (*24–26*). However, none of these tracers can form stable complexes with ^{64}Cu or ^{67}Cu. Despite the high labeling yields of PSMA-617 with ^{64}Cu in vitro (>99%), a poor in vivo stability with high liver uptake was observed (*27,28*).

The pair ^{64}Cu/^{67}Cu is a seamless theranostic match. Because of its favorable properties, ^{64}Cu is ideally suited for long-term PET imaging and allows the dosimetry of tracers labeled with ^{67}Cu to be determined. The therapeutic nuclide ^{67}Cu may be cyclotron-produced and thus available for good-manufacturing-practice production. ^{64}Cu has been shown to be an attractive radionuclide for PET imaging, and a series of PSMA-binding tracers has been described by the Pomper group (*29*). Further examples of previous publications that describe copper-labeled radiotracers for the targeting of PSMA-expressing tumors are ^{64}Cu-NODAGA-PSMA and ^{64}Cu-ABN-1. The Maecke group made a comprehensive preclinical comparison of ^{64}Cu-NODAGA-PSMA to several alternative tracers (*30*), and subsequently, clinical studies with ^{64}Cu-NODAGA-PSMA were published (*31*). As an alternative to the urea-based PSMA-binding tracers, ^{64}Cu-ABN-1 represents a phosphoramidate-based tracer (*32*).

Because of its decay characteristics (half-life, 12.7 h; β^+, 17.4% [E_{max}, 0.656 MeV]; β^-, 39% [E_{max}, 0.573 MeV]), imaging with ^{64}Cu is associated with a comparatively high radiation dose, and PET images obtained with ^{64}Cu do not reach the quality of those obtained with ^{68}Ga (half-life, 67.71 min; β^+, 88.9%) or ^{18}F (half-life, 109.77 min; β^+, 96.7%). The particular strengths of ^{64}Cu lie in its role as the diagnostic nuclide of the matched pair ^{64}Cu/^{67}Cu for theranostic applications. Moreover, the long half-life of ^{64}Cu provides an advantage for imaging at later time points with potentially increased tumor delineation (*33,34*). Furthermore, the half-life of ^{64}Cu offers the logistic advantage of decentralized radiotracer production (*35*).

Here, we describe the preclinical characterization of 9 newly developed copper-labeled PSMA ligands, with the aim of ensuring the advantages of the basic structure of PSMA-617 with a new and stable chelator ensuring the labeling of copper radioisotopes.

A stable and kinetically inert in vivo suitable chelator for copper isotopes will enable the development of promising theranostic radiotracers. In this study, we synthesized and characterized 2 chelators: 4-[(1,4,8,11-tetraazacyclotetradec-1-yl)-methyl]-benzoic acid (a bifunctional macrocyclic cyclam analog) and 4-carboxymethyl-11-(1,3-dicarboxypropyl)-1,4,8,11-tetraazabicyclo[6.6.2]hexadecanepentanedioic acid (a cross-bridged cyclam derivative). These chelators were conjugated either via 2-naphthyl-L-alanine or via 2-naphthyl-L-alanine and the additional spacer 4-aminomethyl-(cyclohexane)carboxylic acid (Fig. 1).

In vivo experiments, such as PET imaging and biodistribution studies, were performed to evaluate the binding characteristics and pharmacokinetic properties of these ligands.

MATERIALS AND METHODS

Solvents and chemicals were purchased from Merck or Sigma-Aldrich and used without further purification. The in vitro experiments were conducted in triplicate, and at least 3 independent sets of data were obtained for each experiment performed. PET imaging of the prostate cancer patient was performed with the consent of the University Hospital Heidelberg following German laws vigorously and in accord with the Helsinki Declaration (permit S321/2012).

Synthesis of the Chelator Moieties

The chelator moieties were synthesized in high yields and characterized by liquid chromatography–mass spectrometry. The synthesis of the chelator 4-[(1,4,8,11-tetraazacyclotetradec-1-yl)-methyl]-benzoic acid was described by Studer and Kaden (*36*), whereas 4-carboxymethyl-11-(1,3-dicarboxypropyl)-1,4,8,11-tetraazabicyclo[6.6.2]hexadecanepentanedioic acid was reported by Boswell et al. (*37*).

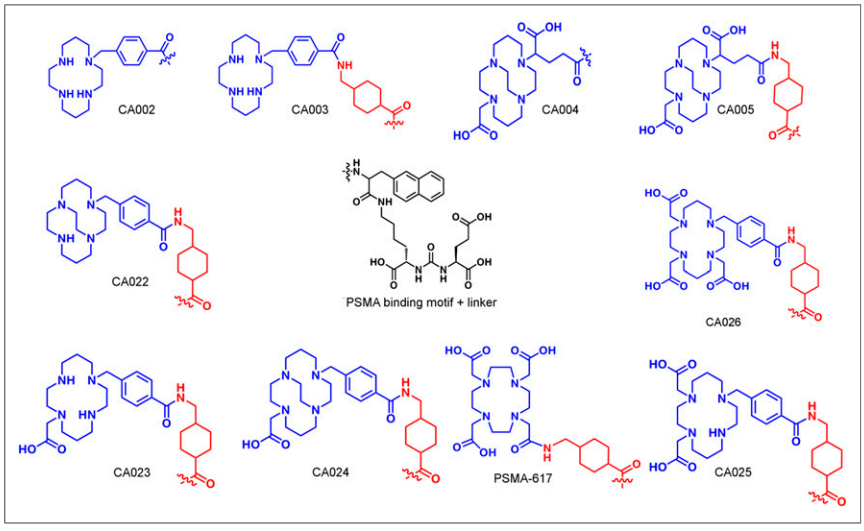

FIGURE 1. Chemical structures of ligands suitable for copper labeling and reference ligand PSMA-617.

Synthesis of PSMA Ligands for Radiolabeling with Radioactive Copper Nuclides

The peptidomimetic glutamate-urea-lysine binding motif and the linker moiety were synthesized by solid-phase peptide chemistry as previously described by Eder et al. (*5*) and Benešová et al. (*6*). The synthesis, including conjugation of the chelator, is described in detail in the supplemental information (supplemental materials are available at http://jnm.snmjournals.org). In brief, the PSMA-binding motif was prepared by solid-phase synthesis on a 2-chlorotrityl resin. The synthesis started with the formation of the isocyanate of the glutamyl moiety using triphosgene. A resin-immobilized (2-chlorotrityl resin), ε-allyloxycarbonyl–protected lysine was added and reacted for 16 h with careful agitation, resulting in the allyloxycarbonyl-protected urea binding motif. The resin was filtered off, and the allyloxycarbonyl-protecting group was cleaved. After coupling of the Fmoc-2-naphthylalanine

and reaction with *trans*-4-(Fmoc-aminomethyl)cyclohexanecarboxylic acid, the chelator was attached. The compound was cleaved from the resin and analyzed by high-performance liquid chromatography (HPLC) and liquid chromatography–mass spectrometry. The crude products were purified by HPLC on a Chromolith SemiPrep column using a linear gradient elution from 0.1% trifluoroacetic acid in water to 0.1% trifluoroacetic acid in acetonitrile. The desired products were analyzed by HPLC (0–100% acetonitrile in water containing 0.1% trifluoroacetic acid) within 5 min on a monolithic reverse-phase column (100 × 3 mm) and by liquid chromatography–mass spectrometry. The product fractions were pooled and lyophilized to obtain the targeting moiety in good yield (~40%).

Radiochemical Synthesis of ^{64}Cu-PSMA Derivatives

The conjugates (1 mM in water, 5 μL, 5 nmol) were added to a mixture of 400 μL of sodium acetate buffer (0.4 M in water, pH 5.0), 10 μL of ascorbic acid (20% in water), and 282 μL of $^{64}CuCl_2$ (DSD Pharma) in 0.1 M HCl (200 MBq). The mixture was heated at 95°C for 5 min. The checked pH of the labeling solution for all compounds was between 4 and 5. The labeling was controlled by radio-HPLC (0–100% acetonitrile in 5 min, monolithic column), with a flow rate of 2 μL/min.

In Vitro Experiments

Cell Culture. The competitive assay was performed using the PSMA-positive C4-2 cell line, a subline of the LNCaP (human lymph node carcinoma of the prostate) cell line (CRL-3314; American Type Culture Collection). The cells were cultivated in Roswell Park Memorial Institute 1640 medium (PAN Biotech) supplemented with 10% fetal calf serum and stable glutamine (PAN Biotech). Cells were grown at 37°C and incubated with humidified air equilibrated with 5% CO_2.

Competitive Cell-Binding Assay. At first, a MultiScreen$_{HTS}$-DV filter plate was coated at room temperature with 100 μL of phosphate-buffered saline (PBS) containing 1% bovine serum albumin per well for 30 min. Afterward, the PBS/bovine serum albumin solution was removed and 1 × 10^5 C4-2 cells in Opti-MEM (Life Technologies Corp.) were added to each well. The inhibitory potency of the synthesized compounds was determined using 0.75 nM of ^{68}Ga-labeled PSMA-HBED-CC dimer (^{68}Ga-PSMA-10) (*38*) as a standard. All nonlabeled compounds were dissolved in Opti-MEM at the following concentrations: 0, 0.5, 1, 2.5, 5, 10, 25, 50, 100, 500, 1,000, and 5,000 nM. This mixture was incubated at 37°C for 45 min. Afterward, the cells were washed twice with PBS on a multiscreen vacuum manifold (Millipore) and the cell-bound radioactivity was measured with a γ-counter (Packard Cobra II; GMI). The 50% inhibitory concentration was calculated using a nonlinear regression algorithm (Graph Pad Prism 5.01 software). The experiments were performed in quadruplicate.

Determination of Internalization Ratio

To determine the specific internalization ratio, two 24-well plates were coated with 0.1% poly-L-lysine in PBS for 20 min at room temperature and then washed once with PBS. Then, 1 mL of Roswell Park Memorial Institute medium containing 10^6 C4-2 cells was added to each well and incubated overnight. The conditions during the experiment for each compound were 37°C and 4°C for incubation with and without, respectively, receptor blocking with 2-(phosphonomethyl)pentanedioic acid (Axxora) at a final concentration of 500 μM. Afterward, the cells in each well were incubated with 250 μL of a 30 nM solution of the ^{64}Cu-labeled compounds. The plates were incubated for 45 min in a water bath at 37°C or on ice at 4°C. Subsequently, the cells were washed 3 times with 1 mL of ice-cold PBS and incubated with 0.5 mL of glycine (50 mM) in HCl, pH 2.8, for 5 min. After an additional washing step with 1 mL of ice-cold PBS, the cells were lysed with 0.5 mL of 0.3 M NaOH, collected, and measured for radioactivity with a γ-counter for 1 min. All experiments were performed in triplicate.

The serum stability was determined by instant thin-layer chromatography (ITLC) and HPLC analysis after radiolabeling of the compounds. A 50-μL (20 MBq) volume of the ^{64}Cu-labeled ligands was added to 200 μL of human serum (H4522; Sigma-Aldrich) and incubated at 37°C for different time points (0, 2, 24, 48, and 72 h). Strips of ITLC silica-gel glass microfiber chromatography paper (0.5 × 5 cm; Agilent Technologies) were used. A 0.5-μL volume of the radiolabeled complex in serum was applied to each strip at 1 cm from the bottom (origin), and the solvent (1% sodium-ethylenediaminetetraacetic acid, pH 4) front was allowed to rise to 5 cm from the bottom. Finally, each strip was cut into 8 pieces, and each piece was measured in a γ-counter.

For HPLC analysis, an equal volume of acetonitrile was added to the samples to precipitate the serum proteins. Subsequently, the samples were centrifuged for 10 min at 13,000 rpm, the pellet and supernatant were separated, and the relative activity was measured. The results are expressed as a percentage. In addition, an aliquot of the supernatant was analyzed by radio-HPLC (0%–100% acetonitrile in 5 min, monolithic column) with a flow rate of 2 mL/min.

In Vivo Characterization

The in vivo experiments were performed in accordance with the laws of the German Federal Republic. For PET imaging and biodistribution studies, male nude mice (BALB/c *nu/nu* mice, 19–23 g) were obtained from Charles River at 4–5 wk old and kept under specific pathogen-free conditions for 1 wk before the study. The mice were housed with a 12-h/12-h light/dark cycle and had free access to water and food. They were anesthetized with 2% sevoflurane and inoculated subcutaneously on the right trunk with 5 × 10^7 C4-2 cells in 50% Matrigel (Corning) in Opti-MEM I (1×) medium. Organ distribution studies were performed when the tumors were approximately 1 cm^3.

Stability in Blood

The stability of ^{64}Cu-labeled CA003 in vivo was determined by ITLC and HPLC. Male BALB/c nude mice without tumor (n = 3) were injected via the tail vein with ^{64}Cu-CA003 (3.6 MBq; 0.26 nmol, dissolved in a total volume of approximately 100 μL of 0.9% saline), and 800 μL of blood were harvested 10 min after injection. The blood sample was centrifuged for 10 min at 13,000 rpm. Subsequently, the pellet and supernatant were separated and the relative activity was determined. ITLC was performed to assess the stability of the radiolabeled compound in the blood as described above. Furthermore, an aliquot of the supernatant was analyzed by radio-HPLC (0%–100% acetonitrile in 5 min, monolithic column) with a flow rate of 2 mL/min after addition of an equal volume of acetonitrile and removal of the proteins by centrifugation.

In Vivo Fate of ^{64}Cu-Chloride and ^{64}Cu-CA003

The metabolization in vivo was studied by radio-HPLC analysis. Female Swiss mice (n = 3) without tumor were injected via the tail vein with ^{64}Cu-chloride (10 MBq in approximately 100 μL of 0.9% saline) or ^{64}Cu-CA003 (9 MBq, 0.30 nmol in approximately 100 μL of 0.9% saline). PET imaging was performed 10 min after injection, and subsequently, blood, the liver, and the kidneys were harvested. The tissues were rinsed with precooled saline, blotted dry, and treated with 2 mL of 0.1 M NH_4OAc/EtOH (35:65). The tissues were homogenized using an Ultra-Turrax T8 (IKA Labortechnik). The samples were centrifuged for 10 min at 13,000 rpm (4°C). Subsequently, the pellet and supernatant were separated and the relative activity was measured. The results are expressed as a percentage. Additionally, an aliquot of supernatant was prepared for HPLC measurement by precipitation of the proteins with acetonitrile as described above. The sample was analyzed by radio-HPLC (0%–100% acetonitrile in 5 min, monolithic column) with a flow rate of 2 mL/min. Fractions were collected every 10 s over the whole course of the chromatography, and the relative activity of the samples was measured in a γ-counter to reconstruct a chromatogram.

Biodistribution Studies

On the basis of the PET results, CA003, the most promising compound, was chosen for a biodistribution study on the C4-2 tumor–bearing mice. Experiments were performed in triplicate. The ^{64}Cu-labeled compound (0.025 nmol; 1 MBq per mouse in approximately 100 μL of 0.9% saline) was administered by tail vein injection. At 10 min, 1 h, 4 h, 24 h, and 72 h, the organs were dissected and weighed and the activity was measured using a γ-counter (Packard Cobra Auto-Gamma). The percentage injected dose per gram (%ID/g) was calculated.

Dynamic and Static PET Scans

For small-animal PET imaging with various ^{64}Cu-labeled PSMA ligands, 0.2 nmol (10 MBq) of the radiolabeled compound in approximately 100 μL of 0.9% saline was injected into a C4-2 tumor–bearing mouse. Dynamic imaging was performed in a small-animal PET scanner (Siemens Inveon D-PET). SUVs were obtained from conventional (nondynamic) PET images as follows:

$$\mathrm{SUV} = \frac{\text{activity in ROI } \left(\frac{\mathrm{Bq}}{\mathrm{mL}}\right) \times \text{animal weight (g)}}{\text{injected dose (Bq)}}.$$

Volumes of interest were obtained by manual delineation of the appropriate whole tissue (heart, kidneys, bladder, and tumor, with an approximate volume of 0.1–0.5 cm^3, or portions of liver and muscle tissue). Images were reconstructed using an ordered-subsets expectation maximization 3-dimensional/shifted Poisson maximum a posteriori algorithm with 16 subsets, 2 iterations, and an image x–y size of 256 and z size of 161. The data were not modified with a postprocessing filter. The software used to analyze images and time–activity curves was Inveon Acquisition Workplace from Siemens Inveon Research Workplace 4.1. Dynamic PET scans were performed 0–60 min after injection, and images were reconstructed in 3 time frames of 20 min (0–20, 20–40, and 40–60 min) for visual display. For some compounds that showed long retention, later time points (2, 4, 20, and 45/48 h) were included as shown in Figures 2 and 3 and Supplemental Tables 1 and 2. After 1 h, a static PET scan was generated. To compare the different radiotracers, the mean SUVs were plotted over time.

Biodistribution in Human PET Scan

Imaging with CA003 was performed as previously described by Afshar-Oromieh et al. (*39*). Images were obtained with ^{64}Cu-CA003, which was applied by intravenous injection (200 MBq and 5 nmol of ligand). The diagnostic examination of ^{64}Cu-CA003 was conducted at 2 and 20 h after injection, whereas for PSMA-617 the time points were 1 and 3 h. The activity distributions of the source organs were determined with standard clinical software (Syngo; Siemens), which was used to define the volumes of interest in the PET images.

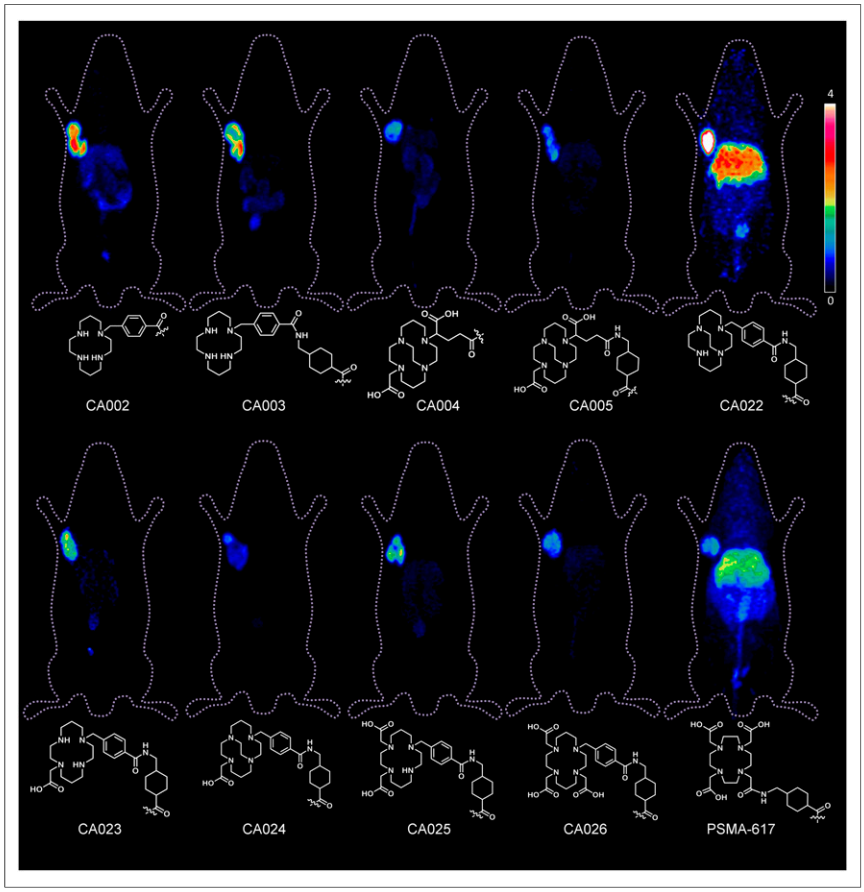

FIGURE 2. Whole-body small-animal PET scans as maximum-intensity projections of ^{64}Cu-labeled compounds in BALB/c *nu/nu* C4-2 tumor–bearing mice 24 h after injection via tail vein. Tumor-targeting efficacy and pharmacokinetic properties were evaluated by injection of 0.2 nmol (~10 MBq, 100 μL as injected volume of 0.9% saline) of labeled compounds. Color bar gives link between SUV and color scale of PET image.

RESULTS

Synthesis of the binding motif containing the linkers 2-naphthyl-L-alanine and cyclohexanecarboxylic acid was followed by coupling of various chelators. After cleavage from the resin and purification by HPLC, the conjugates were obtained in yields of approximately 40% at a purity of 95% as determined by HPLC. The results of the syntheses are summarized in Table 1.

Radiolabeling

Radiolabeling of 0.2 nmol of the precursor at 95°C with ^{64}Cu led to yields of more than 98% within 10 min (as illustrated by the radiochromatograms in Supplemental Fig. 25). The specific activity of ^{64}Cu-PSMA-CA003 was approximately 40 MBq/nmol. The same protocol was used for the labeling with ^{67}Cu.

Competitive Cell Binding Internalization Ratios and Serum Stability

C4-2 cells, a subline of the PSMA-expressing cell line LNCaP, were used for analyzing the competitive cell binding. Determination of the equilibrium inhibition constant (K_i) showed nanomolar binding affinities for the synthesized ligands to PSMA. As shown in Table 2, CA003 revealed the highest affinity to PSMA, followed by CA005, CA002, and CA026. Moreover, the ^{64}Cu-labeled compounds showed specific binding to C4-2 cells. The internalized percentages were 34.63% ± 2.77% for

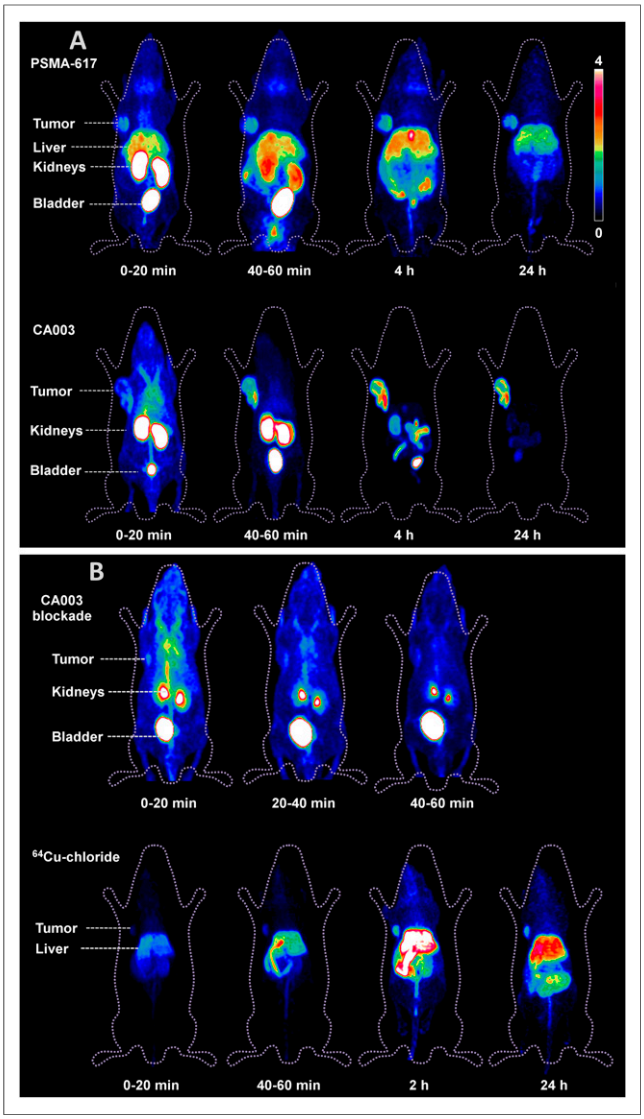

FIGURE 3. Whole-body small-animal PET scans as maximum-intensity projections of BALB/c *nu/nu* mice bearing C4-2 tumor xenografts. (A) ^{64}Cu-PSMA-617 (10 MBq, 0.2 nmol) and ^{64}Cu-CA003 (10 MBq, 0.2 nmol). (B) ^{64}Cu-CA003 (5 MBq, 0.030 nmol) coinjected with excess of nonlabeled PSMA-617 (2 mg/kg of body weight) and ^{64}Cu-chloride (10 MBq). Color bar gives link between SUV and color scale of PET image.

^{64}Cu-CA003, 18.63% ± 4.46% for ^{64}Cu-CA005, and 38.7% ± 6.69% for ^{64}Cu-CA022 (n = 3). These experiments used 10^6 C4-2 cells (Table 2).

The stability of all compounds was determined in human serum. Supplemental Figure 19 graphically expresses the results for 3 main compounds: CA003, containing the chelator (4-[(1,4,8,11-tetraazacyclotetradec-1-yl)-methyl]benzoic acid (CTPA); CA005, containing a cross-bridged chelator; and PSMA 617, containing an unmodified DOTA chelator. The compounds were radiolabeled with ^{64}Cu and incubated for 72 h in human serum. Stability was assessed by ITLC and HPLC. Up to 2 h of incubation, ITLC showed that the degree of dissociation for all compounds was less than 2% ± 0.6%. After 24 h of incubation, only 6% ± 4% of ^{64}Cu-CA003 and 3% ± 1% of ^{64}Cu-CA005 were dissociated. In contrast, ^{64}Cu-PSMA-617 showed 13% ± 3% free ^{64}Cu activity.

Long-term stability examination at 72 h showed that ^{64}Cu-CA005 (8% ± 4%) possesses stability comparable to ^{64}Cu-CA003 (11% ± 3%). At that time, 18% ± 6% of ^{64}Cu-PSMA-617 was dissociated. After incubation for 2 h, measurement of pellet activity (Supplemental Fig. 20) revealed that 19.0% ± 5.2% of ^{64}Cu-CA003, 12% ± 7.2% of ^{64}Cu-CA005, and 40% ± 7.5% of ^{64}Cu-PSMA-617 was precipitated with the protein fraction. The percentage of activity in the pellet increased over time. Activity in the pellet was highest for ^{64}Cu-PSMA-617, followed by ^{64}Cu-CA003 and then ^{64}Cu-CA005.

In Vivo Characterization

In vivo stability was determined by ITLC and HPLC after PET imaging (Supplemental Fig. 23) using blood harvested 10 min after injection. ITLC results for blood stability showed that ^{64}Cu-CA003 undergoes 3% ^{64}Cu dissociation, or 97% ± 2.3% of the intact tracer. Radio-HPLC showed that the activity elutes at the retention time of intact tracer, confirming the integrity of the copper complex (Supplemental Fig. 24). The in vivo fate was determined by PET imaging, which showed ^{64}Cu-chloride and ^{64}Cu-CA003 to have different pharmacokinetics (Supplemental Fig. 21). Maximum-intensity projections indicated ^{64}Cu-chloride to have lower blood circulation (1.3 vs. 2.3), higher liver uptake (2.7 vs. 1.0), and lower kidney uptake (3.4 vs. 5.7) than ^{64}Cu-CA003 (Supplemental Fig. 21). The integrity of the ^{64}Cu-CA003 was proven by radio-HPLC chromatograms of tissue extracts of kidney, blood, and liver (Supplemental Fig. 23). The chromatogram for ^{64}Cu-CA003 showed its retention time to be different from that of free copper (^{64}Cu-chloride) (Supplemental Fig. 24).

Organ Distribution and Small-Animal PET Imaging

The biodistribution results for ^{64}Cu-CA003 (n = 3) are presented in Figure 4 and Supplemental Table 3. The organ distribution at 10 min, 1 h, 4 h, 24 h, and 72 h after injection is shown, as well as the results of the experiment in which PSMA-617 was simultaneously administered to block PSMA binding at 1 h (n = 3). Ten minutes after injection, tumor uptake was 11.33 ± 4.11 %ID/g. After 4 h, tracer accumulation was much higher in tumors (32.34 ± 10.6 %ID/g) than in the kidneys (13.33 ± 3.36 %ID/g). Time–activity curves generated from the dynamic PET imaging showed a tumor-to-muscle ratio of 10.5 and a tumor-to-blood ratio of 3.0 at 1 h after injection (Supplemental Table 1). These curves indicate rapid renal uptake. The organ distribution study (Fig. 4; Supplemental Table 3) showed that the high kidney uptake at 1 h (67.04 ± 20.89 %ID/g) was largely cleared within 24 h (7.48 ± 8.51 %ID/g). In contrast, the high tumor uptake at 1 h (30.83 ± 12.61 %ID/g) remained almost constant at 24 h (19.99 ± 6.43 %ID/g). PET imaging confirmed strong accumulation of radiotracer in tumors (Fig. 3). At 1 h after injection, background radioactivity in organs such as the kidneys decreased whereas the tumor-to-background ratio increased. At 24 h after injection, the PET scans demonstrated high tumor uptake confirming enrichment in the tumor (Fig. 2). The high uptake was retained even at 45 h after injection (Fig. 3).

The specificity of binding to PSMA was proven with a blockade experiment: coinjection of nonlabeled PSMA-617 (2 mg/kg) strongly decreased the accumulation of ^{64}Cu-CA003 in C4-2 tumors (from 30.83 ± 12.61 %ID/g to 2.35 ± 0.38 %ID/g) and in the kidneys (from 67.04 ± 20.89 %ID/g to 3.47 ± 0.48 %ID/g) at 1 h after injection. PET imaging of ^{64}Cu-CA003 with an excess of nonlabeled PSMA (Fig. 4B; Supplemental Fig. 3) clearly confirmed the biodistribution results.

TABLE 1
Analytic Data of Copper Ligands

Compound	Molecular weight (g/mol)	[^{64}Cu-ligand]-HPLC retention time (min)	m/z*experimental
CA002	832.45	2.39	833.42
CA003	971.55	2.37	972.51
CA004	912.46	2.38	913.60
CA005	1,051.56	2.61	1,052.53
CA022	997.56	2.71	998.53
CA023	1,029.55	2.59	1,030.53
CA024	1,055.57	2.66	1,056.54
CA025	1,087.56	2.58	1,088.53
CA026	1,145.56	2.58	1,146.53

*Mass spectrometry of nonlabeled ligands detected as $[M + H]^+$.

Comparison of ^{64}Cu-CA003 to ^{64}Cu-PSMA-617 and ^{64}Cu-Chloride In Vivo

To prove the in vivo stability of the copper complexes of PSMA-CA003, we compared ^{64}Cu-CA003 with ^{64}Cu-PSMA-617 and with ^{64}Cu-chloride (Fig. 3). The compounds were studied in a small-animal dynamic PET study on a C4-2 tumor xenograft The time–activity curves for ^{64}Cu-CA003 showed a high tumor-to-liver ratio of 4.0 at 1 h after injection, whereas for ^{64}Cu-PSMA-617 the tumor-to-liver ratio was 0.37 (Fig. 3 and Supplemental Tables 1 and 2). To prove that the species taken up into the tumor is actually ^{64}Cu-CA003 and not free ^{64}Cu, PET imaging of ^{64}Cu-chloride on C4-2 tumor–bearing mice (Fig. 3) was followed by homogenization, extraction, and subsequent HPLC analysis of the respective tissue. The pharmacokinetic observed for ^{64}Cu-chloride was different from that for ^{64}Cu-CA003. PET maximum-intensity projections of ^{64}Cu-chloride revealed tumor uptake to be increasing for up to 2 h after injection. In contrast to ^{64}Cu-CA003, ^{64}Cu-chloride showed a high liver accumulation (Fig. 3). The tumor-to-liver ratio at 2 h was 0.38 for ^{64}Cu-chloride but 6.3 for ^{64}Cu-CA003.

TABLE 2
PSMA Inhibition Potencies (Expressed as K_i) and Specific Internalization Values

Compound	K_i (nM)	Specific cell surface	Specific lysate
CA002	1.9 ± 0.70	48 ± 3.9	16 ± 2.4
CA003	1.6 ± 0.52	94 ± 6.9	35 ± 2.8
CA004	15 ± 0.89	45 ± 3.4	13 ± 2.2
CA005	1.8 ± 0.65	41 ± 4.3	19 ± 4.5
CA022	12 ± 2.0	123 ± 22	39 ± 6.7
CA023	14 ± 2.0	103 ± 6.6	28 ± 8.7
CA024	21 ± 4.0	35 ± 5.8	8.6 ± 7.0
CA025	14 ± 1.7	68 ± 11	16 ± 8.0
CA026	4.4 ± 1.6	96 ± 16	24.5 ± 14
PSMA-617	2.3 ± 2.9	45 ± 3.6	15 ± 3.0

Data are mean ± SD (n = 3). Internalization is expressed as percentage injected activity per 10^6 cells.

PET Imaging of ^{64}Cu-CA003 in a Human

To show the clinical applicability of ^{64}Cu-CA003, a PET scan in a first patient with a high serum prostate-specific antigen value (185 ng/mL; reference range < 4 ng/mL) and lactate dehydrogenase (861 U/L; reference range < 342) was performed. The resulting PET image is presented in Figure 5. It shows that uptake of the PSMA ligand is higher in tumor than in several commonly used reference tissues such as liver and salivary glands. The obtained SUVs were comparable to literature values for PSMA-617 (*26*), the current standard of reference for theranostic PSMA ligands (Table 3). Because the acquisition was with standard scanner settings, calibrated for pure positron emitters such as ^{18}F, the additional γ-lines emitted by ^{64}Cu presumably increase the number of random coincidences, thus systematically overestimating SUVs quantitatively. However, at the early image time-point 2 h after injection, the SUV ratios between CA003 and PSMA-617 are almost equal for both tumor lesions and reference tissues, indicating that the diagnostic performance regarding tumor delineation may be similar at day 1 examinations. As reflected by the values obtained with ^{64}Cu-CA003 at 2 h versus 20 h after injection, unspecific uptake in normal organs is characterized by a strong washout. In contrast, tumor values reveal a relatively stable accumulation of the radiopharmaceutical, and delayed images—which can be obtained with ^{64}Cu, having a 12.7-h half-life, but not with the 1-h half-life of ^{68}Ga—may further improve tumor delineation. Rapid nontumor clearance is also an excellent prerequisite for potential therapeutic application. However, hepatobiliary clearance can cause some hot spots inside the intestine in later imaging, requiring more thorough reading to distinguish these from peritoneal or mesenteric lymph nodes.

DISCUSSION

The main purpose of this study was to develop novel PSMA-specific ligands that form stable complexes with copper radioisotopes. Among 9 compounds investigated, CA003 was the most promising. Here, we report the preclinical characterization of CA003 and a first application in a patient. The syntheses of the precursor molecules and their chelator derivatives were accomplished by solid-phase methods. The ^{64}Cu labeling of the PSMA ligands could be performed in quantitative yields. The urea-based binding motif Lys-NH-CO-NH-Glu has been shown to bind to

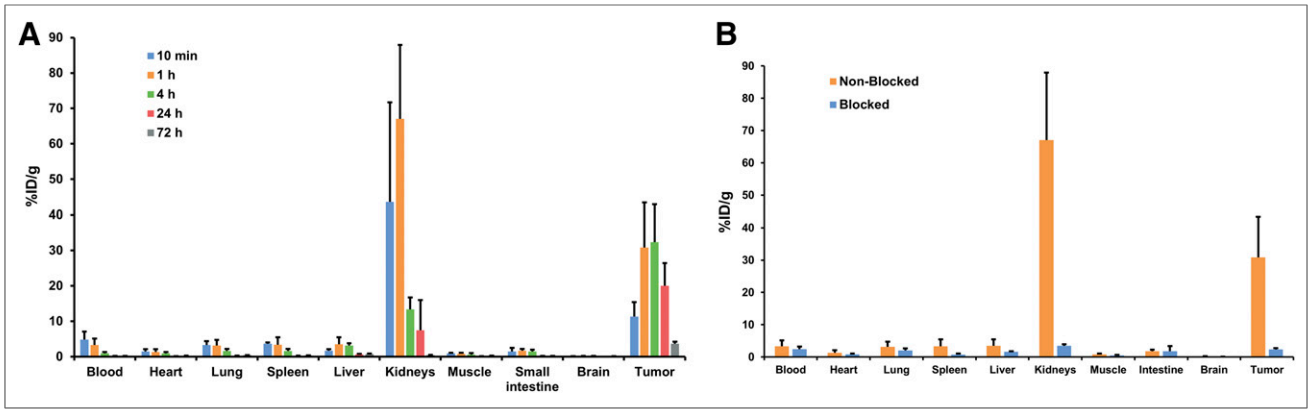

FIGURE 4. (A) Organ distribution of 0.025 nmol of ^{64}Cu-CA003 at 10 min, 1 h, 4 h, 24 h, and 72 h after injection. Values are range of %ID/g of tissue ± SD; $n = 3$ for all tissues. (B) In blockade experiment, ^{64}Cu-CA003 (0.030 nmol) was injected at same time as 2 mg of PSMA-617 per kilogram of body weight.

PSMA with high affinity (*22,23*), and lipophilic linkers further optimize its binding properties (*26,40*). In the first instance, the chelator moiety was chosen with respect to its influence on the pharmacokinetics. It has already been reported that small, nonpolar substituents such as the aromatic moiety in MIP-1466 (*41*) lead to compounds with a pharmacokinetic that is substantially different from PSMA-617. Unmodified cyclam is a substituent that comes close to these prerequisites. Interestingly, CA003 fulfilled the expectations and showed extended retention in the circulation, displaying characteristics of the albumin-binding tracers recently described by Benešová et al. (*42*). In the present study, the high inhibition potency of the synthesized ligands, in particular CA003 (K_i = 1.60 ± 0.52 nM), was demonstrated, as well as the high specific uptake in the PSMA-positive C4-2 cells. Among all compounds, ^{64}Cu-CA003 showed high specific internalization of 34.63% ± 2.77% injected activity/10^6 cells. In CA003, the chelator CTPA, which is linked via a benzyl group, leads to a hydrophilicity and net charge that provide ideal pharmacokinetic properties.

When compared with their non–cross-bridged counterparts, the in vitro and in vivo stability of the Cu(II) cross-bridged macrocycle complexes may be explained in part by differences in their coordination chemistry. The structures of the Cu(II) complexes of TETA and CB-TE2A possess differences despite their related frameworks (*43*). Cu(II)-CB-TE2A complex has an octahedral complex with 2 axial nitrogens, 2 equatorial nitrogens, and carboxylate groups at the remaining 2 *cis*-equatorial positions as particular features (*44*). Cu(II)-TETA forms a distorted octahedron with 2 weakly coordinated axial carboxylates, whereas the 4 nitrogens of the tetraazamacrocycle are at equatorial positions (*45*). The 2 complexes have different overall charges. Cu(II)-CB-TE2A forms a neutral complex, completely enveloping the Cu(II) cation, whereas Cu(II)-TETA has an overall −2 charge due to 2 free carboxylates (*43*). The structure of the Cu(II)-DOTA complex is analogous to that of Cu(II)-TETA (*45,46*). However, metabolism experiments confirmed that ^{64}Cu-DOTA underwent more transchelation to liver protein than ^{64}Cu-TETA (*43*).

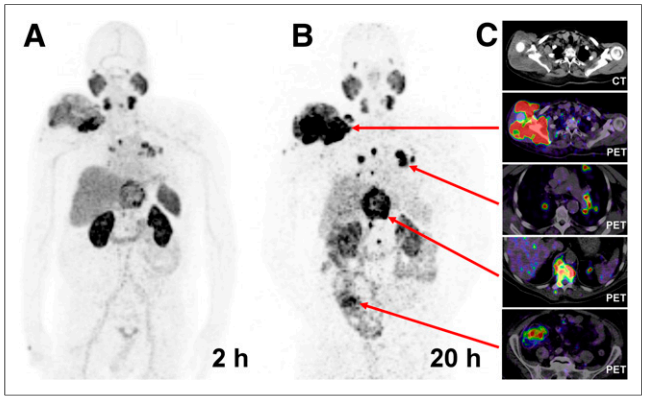

FIGURE 5. (A and B) ^{64}Cu-CA003 (200 MBq, 0.5 nmol) PET/CT maximum-intensity projections of patient at 2 h (A) and 20 h (B) after injection. Arrows point to selected right shoulder soft-tissue infiltration originating from scapula, lung, bone, and lymph node metastases, increasing in contrast over time. Hepatobiliary clearance causes hot spots inside intestine in delayed imaging. (C) Cross-sectional slices are mandatory to avoid false-positive readings.

TABLE 3
Safety Dosimetry Estimate of Diagnostic ^{64}Cu-CA003 and ^{68}Ga-PSMA-617* Based on Male Adult Phantom in OLINDA

Organ	^{64}Cu-CA003 SUV_{mean}		^{68}Ga-PSMA-617 SUV_{mean}	
	After 2 h	After 20 h	After 1 h	After 3 h
Lacrimal gland	9.9	4.1	4.9	5.9
Nasal mucosa	4.5	2.3	2.9	3.4
Parotid gland	15.4	5.1	10.4	13.1
Submandibular gland	19.9	4.4	10	12.4
Sublingual gland	11.2	2.6	4.6	4.0
Blood pool, mediastinal	3.6	0.4	2.5	2.4
Liver	6.0	0.8	3.3	2.7
Spleen	10.6	0.7	4.3	3.5
Proximal small intestine	12.3	2.4	4.7	5.5
Colon	4.6	2.9	3.5	4.0
Kidneys	19.0	4.9	15.6	17.0
Gluteal muscle	0.6	0.1	0.7	0.7
Bone metastases	24.2	15.7	9.4	6.27
Lymph node	16.8	11.3	7.1	13.54

*Afshar-Oromieh et al. (*39*).

The results obtained from the serum stability experiment confirmed that—besides the DOTA-containing compounds, such as PSMA-617—all compounds showed high serum stability within the observation period of 24 h. Although the compounds containing the cross-bridged chelators showed slightly enhanced serum stability (*43*), there is experimental proof that even unmodified CTPA shows high serum stability, which is in accordance with our stability examinations (*47*). Furthermore, CTPA has previously been used for antibody labeling with ^{67}Cu (*47*). Considering the rapid targeting of small PSMA-binding molecules, the CTPA conjugates deserved investigation.

The organ distribution results of ^{64}Cu-CA003 exhibited high tumor–to–normal-tissue ratios that increased over time, thereby providing images with high contrast. Moreover, no bone uptake was observed for CA003, indicating that this agent could be applied for the detection of prostate cancer metastases in bone tissue. In the pharmacokinetic investigation, both kidney and tumor uptake of ^{64}Cu-CA003 could be specifically blocked by an excess of PSMA-617. Imaging and biodistribution studies demonstrated higher in vivo stability for this compound even without using cross-bridge chelators. The high tumor accumulation and the kidney clearance for ^{64}Cu-CA003 were significantly improved in comparison with literature values for ^{68}Ga-PSMA-11, ^{68}Ga-PSMA-617, and ^{18}F-PSMA-1007 (*6,7,48*).

PSMA is also expressed in the kidneys (*49*). Nevertheless, we noted high accumulation in kidney only at the renal perfusion/filtration phase soon after intravenous injection. A difference in PSMA-specific binding between tumor lesions and the kidneys has already been observed previously. It is thought to result from reduced internalization of renal PSMA after binding to filamin A, glycosylation, splicing variants, and other isoforms (*50*). Because the PSMA expressed by the LNCaP xenografts represents the human form of GCP II whereas the kidney PSMA represent the orthologue of mice, it would be premature to conclude that the higher tumor specificity of CA003 will be completely transferable to human.

In the blocking experiments, a strong reduction of kidney retention was observed. It has already been demonstrated that kidney uptake of PSMA ligands can be blocked with monosodium glutamate (*51*). Glutamate has no specific binding to PSMA. However, because of its structural similarity to the Glu-urea motif of PSMA ligands, investigators thought that glutamate could serve as a competitive blocking agent also to nonspecific ion transporters. Figure 3 and Supplemental Figure 1 show that ^{64}Cu-CA003 is excreted in urine. The bladder shows the strongest signal after 60 min (Fig. 3A), and in contrast to radioactivity in the kidneys, which shows saturation after 20 min (Supplemental Fig. 1), radioactivity in urine increases for up to 60 min. We interpret this finding as indicating that ^{64}Cu-CA003 is filtered into urine in a non–PSMA-specific manner and that kidney cells expressing PSMA are not involved in the excretion. This interpretation is emphasized by the blocking experiment in Figure 4B and Supplemental Table 3, in which loss of radioactivity by blocking of PSMA led to increased excretion of copper-labeled CA003.

Generally, high uptake in the liver is assumed to indicate instability of ^{64}Cu complexes in vivo. The high liver accumulation and retention of ^{64}Cu-PSMA-617 in comparison to ^{64}Cu-CA003 indicates significant loss of copper from PSMA-617, as illustrated by the PET images in Figure 3 and the time–activity curves for tumor and liver tissue in Figure 6. The assumption that free copper released from ^{64}Cu-PSMA-617 accounts for the high liver uptake is in accordance with images published by Cai et al. (*52*). Because ^{64}Cu-chloride can also accumulate in prostate cancer lesions, $^{64}CuCl_2$ can be used as a PET tracer to detected prostate cancer (*53*). More recently, Piccardo et al. (*54*) reported that $^{64}CuCl_2$ is more suitable than ^{18}F-choline for exploring the pelvis and prostatic bed. However, in both studies the liver is the critical organ.

Compared with ^{64}Cu-CC34, which contains a NODAGA chelator, ^{64}Cu-CA003 showed longer blood retention, significantly lower kidney uptake, and a higher tumor-to-background ratio. Both compounds showed low liver uptake; however, ^{64}Cu-CC34 demonstrates higher spleen uptake than ^{64}Cu-CA003 (*30*). The ^{64}Cu-labeled phosphoramidate-based PSMA inhibitor ABN-1 (*32*) accumulates mainly in the kidneys. In addition, a substantial amount of ^{64}Cu-ABN-1 was found in the liver, leading to decreased tumor-to-background ratios when compared with ^{64}Cu-CA003. It is important to underline that the high liver uptake can be associated with transchelation and enzymatic degradation by liver enzymes. Earlier PET studies showed ^{64}Cu NODAGA-PSMA to be a promising imaging tool to detect residual disease in patients with recurrent or primary progressive prostate cancer (*31*).

A general comparison of all chelators used in this study is relatively complex. The number and organization of pendant arms use both the macrocyclic and the chelate effects to enhance stability. Increasing the number of pendants does not necessarily increase stability. In addition, other factors, such as the pendant arm length, also contribute to stability (*55*). When comparing nonbridged and bridged cyclam complexes, in some cases nonbridged cyclam complexes have values (stability constant = $\log K_f = 27.1$) similar to those of bridged cyclam complexes ($\log K_{Cu\text{-}L} = 27.1$) (*56*). Moreover, greater geometric constraint incorporated into the macrocyclic ligand enhances the kinetic inertness and thermodynamic stability of copper complexes. Our results suggest that the high kinetic inertness of Cu(II) against decomplexation (proton-assisted, as well as transchelation or transmetallation) might thus be more significant than thermodynamic stability in vivo.

The instability of ^{64}Cu-PSMA-617 in vivo is indicated by the release of poorly

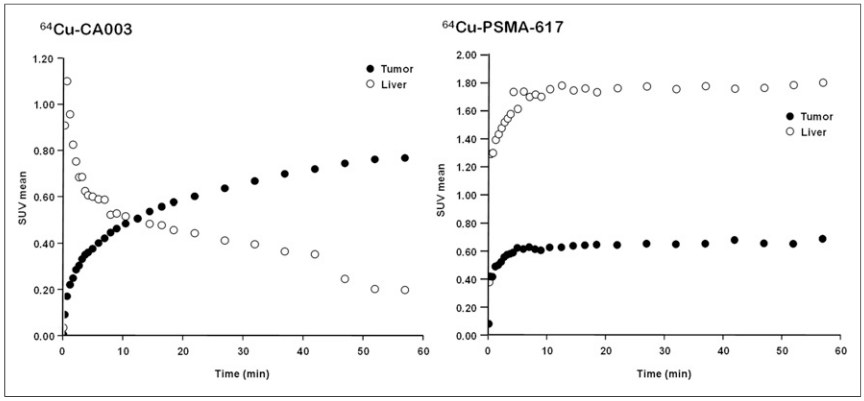

FIGURE 6. Time–activity curves of tumor and liver tissue for ^{64}Cu-CA003 (10 MBq, 0.2 nmol) and ^{64}Cu-PSMA-617 (10 MBq, 0.2 nmol) in BALB/c *nu/nu* mice bearing C4-2 tumor xenografts up to 1 h after injection. Data are SUV_{mean}, and curves are derived from single animal and match results obtained by PET imaging and biodistribution experiments.

coordinated ^{64}Cu into the blood (*57,58*) or by binding to ceruloplasmin (*59*) or to metallothionein or superoxide dismutase (SOD) in the liver (*28,60,61*).

The PET scan of the first patient examined with ^{64}Cu-CA003 demonstrated high tumor accumulation at low background values, comparable to ^{68}Ga-PSMA-617. Thus, the new ligands were explicitly demonstrated to be promising agents to target PSMA-positive prostate tumors.

Because the main goal of this work is the development of therapeutic tracers that protect nontarget organs, the internalization experiments and binding affinities were considered the main first decision criteria. The final decision to focus the studies on ^{64}Cu-CA003 was based on the interplay of properties in the whole broad series of experiments described, in particular the PET imaging and the distribution in the mouse models. Because the relative long half-life of ^{64}Cu benefits shipment and dosimetry studies, ^{64}Cu-labeled ligands might have a theranostic future in combination with the short-range β-emitter ^{67}Cu. One of most relevant characteristics of ^{64}Cu is its low positron energy (653 keV), comparable to that of ^{18}F (633 keV), leading to a similar degree of PET image blurring, which is much less than that of most other PET radionuclides. The reason for the image blurring is the relatively high E_{max} of 580 keV and the high β^- and EC (electron capture) branching amounts of 34% and 44%, respectively, which also increase radiation exposure (*62*). However the accessibility of ^{64}Cu is still limited, resulting in high costs (also caused by the fact that hospitalization of the patients is mandatory). However, despite these limitations, ^{64}Cu represents a valuable alternative to ^{18}F—whose long-distance shipment is not feasible—and offers an advantage for ligands with longer circulating times to achieve good tumor-to-background ratios. Furthermore, one of most plausible applications of ^{64}Cu-labeled compounds is dosimetry studies before radiotherapy with ^{67}Cu-labeled compounds. ^{67}Cu offers several benefits: a half-life of 2.5 d, allowing for optimized dosing combined with only a few days of hospitalization and consequently less costly waste management, as well as lower irradiation of nontarget tissue and a cost and energy equivalent to ^{177}Lu. ^{64}Cu-labeled cetuximab was proposed for integrated treatment and PET-guided surgery in human gastrointestinal cancer xenografts (*63*). Similarly, ^{64}Cu-CA003 might serve as a tracer for radioguided surgery. This technique is currently being established with ^{99m}Tc-PSMA and may benefit from high-resolution PET scans before surgery and from the high tracer retention of ^{64}Cu-CA003 after 24 h (*64*).

Among all synthesized compounds, we suggest CA003, preferentially in combination with ^{67}Cu, as a radiotracer for targeting prostate cancer.

CONCLUSION

The current treatments for prostate cancer come with several side effects that decrease quality of life. Targeted therapy is a new hope for prostate cancer. Of the ^{64}Cu-labeled PSMA-ligands, CA003, CA005, and CA023 proved to be promising for targeting PSMA on prostate tumor cells. We recommend CA003 for the first studies on patients. CA003 demonstrates high potential affinity, high PSMA-specific uptake, fast clearance, and rapid kidney excretion, which are ideal clinical properties for imaging and endoradiotherapy of prostate cancer.

DISCLOSURE

The compounds described are the subject of a patent application by Uwe Haberkorn, José Carlos Dos Santos, Walter Mier, Clemens Kratochwil, Ulrike Bauder-Wüst, Klaus Kopka, and Martin Schäfer. The Richard Winter Foundation supported José Carlos dos Santos with a PhD fellowship. No other potential conflict of interest relevant to this article was reported.

ACKNOWLEDGMENT

We are grateful to Susanne Krämer, from the Department of Nuclear Medicine, Heidelberg University Hospital, for expert assistance with radiolabeling of ^{64}Cu-CA003 for clinical applications.

KEY POINTS

QUESTION: Can the potential of PSMA-binding tracers be applied to copper-labeled tracers?

PERTINENT FINDINGS: Several PSMA-binding ligands containing chelators dedicated for copper complexation were synthesized by solid-phase synthesis and characterized in in vitro and in vivo models. The excellent targeting performance determined in the animal models could be confirmed in a first prostate tumor patient.

IMPLICATIONS FOR PATIENT CARE: The possibility to target PSMA and visualize PSMA-positive tumor lesions with copper isotopes represents the basis to extend the theranostic applications of PSMA-binding tracers.

REFERENCES

1. Silver DA, Pellicer I, Fair WR, Heston WD, Cordon-Cardo C. Prostate-specific membrane antigen expression in normal and malignant human tissues. *Clin Cancer Res.* 1997;3:81–85.
2. Davis MI, Bennett MJ, Thomas LM, Bjorkman PJ. Crystal structure of prostate-specific membrane antigen, a tumor marker and peptidase. *Proc Natl Acad Sci USA.* 2005;102:5981–5986.
3. Abuchowski A, van Es T, Palczuk NC, Davis FF. Alteration of immunological properties of bovine serum albumin by covalent attachment of polyethylene glycol. *J Biol Chem.* 1977;252:3578–3581.
4. Rowe SP, Gorin MA, Allaf ME, et al. PET imaging of prostate-specific membrane antigen in prostate cancer: current state of the art and future challenges. *Prostate Cancer Prostatic Dis.* 2016;19:223–230.
5. Eder M, Schafer M, Bauder-Wust U, et al. ^{68}Ga-complex lipophilicity and the targeting property of a urea-based PSMA inhibitor for PET imaging. *Bioconjug Chem.* 2012;23:688–697.
6. Benešová M, Schafer M, Bauder-Wust U, et al. Preclinical evaluation of a tailor-made DOTA-conjugated PSMA inhibitor with optimized linker moiety for imaging and endoradiotherapy of prostate cancer. *J Nucl Med.* 2015;56:914–920.
7. Cardinale J, Schafer M, Benesova M, et al. Preclinical evaluation of ^{18}F-PSMA-1007, a new prostate-specific membrane antigen ligand for prostate cancer imaging. *J Nucl Med.* 2017;58:425–431.
8. Taneja SS. ProstaScint® scan: contemporary use in clinical practice. *Rev Urol.* 2004;6(suppl 10):S19–S28.
9. Nanus DM, Milowsky MI, Kostakoglu L, et al. Clinical use of monoclonal antibody HuJ591 therapy: targeting prostate specific membrane antigen. *J Urol.* 2003;170(suppl):S84–S88.
10. Scher B, Seitz M, Albinger W, et al. Value of ^{11}C-choline PET and PET/CT in patients with suspected prostate cancer. *Eur J Nucl Med Mol Imaging.* 2007;34:45–53.
11. Hodolic M. Role of ^{18}F-choline PET/CT in evaluation of patients with prostate carcinoma. *Radiol Oncol.* 2011;45:17–21.
12. Chen Y, Pullambhatla M, Foss CA, et al. 2-(3-{1-carboxy-5-[(6-[^{18}F]fluoro-pyridine-3-carbonyl)-amino]-pentyl}-ureido)-pentanedioic acid, [^{18}F]DCFPyL, a PSMA-based PET imaging agent for prostate cancer. *Clin Cancer Res.* 2011;17:7645–7653.
13. Turkbey B, Mena E, Lindenberg L, et al. ^{18}F-DCFBC prostate-specific membrane antigen-targeted PET/CT imaging in localized prostate cancer: correlation with multiparametric MRI and histopathology. *Clin Nucl Med.* 2017;42:735–740.

14. Weineisen M, Schottelius M, Simecek J, et al. ^{68}Ga- and ^{177}Lu-labeled PSMA I&T: optimization of a PSMA-targeted theranostic concept and first proof-of-concept human studies. *J Nucl Med.* 2015;56:1169–1176.
15. Zechmann CM, Afshar-Oromieh A, Armor T, et al. Radiation dosimetry and first therapy results with a ^{124}I/^{131}I-labeled small molecule (MIP-1095) targeting PSMA for prostate cancer therapy. *Eur J Nucl Med Mol Imaging.* 2014;41:1280–1292.
16. Schmidkonz C, Hollweg C, Beck M, et al. ^{99m}Tc-MIP-1404-SPECT/CT for the detection of PSMA-positive lesions in 225 patients with biochemical recurrence of prostate cancer. *Prostate.* 2018;78:54–63.
17. Sathekge M, Knoesen O, Meckel M, Modiselle M, Vorster M, Marx S. ^{213}Bi-PSMA-617 targeted alpha-radionuclide therapy in metastatic castration-resistant prostate cancer. *Eur J Nucl Med Mol Imaging.* 2017;44:1099–1100.
18. Zlatopolskiy BD, Endepols H, Krapf P, et al. Discovery of ^{18}F-JK-PSMA-7, a novel PET probe for the detection of small PSMA-positive lesions. *J Nucl Med.* 2019;60:817–823.
19. Afshar-Oromieh A, Avtzi E, Giesel FL, et al. The diagnostic value of PET/CT imaging with the ^{68}Ga-labelled PSMA ligand HBED-CC in the diagnosis of recurrent prostate cancer. *Eur J Nucl Med Mol Imaging.* 2015;42:197–209.
20. Baranski AC, Schafer M, Bauder-Wust U, et al. Improving the imaging contrast of ^{68}Ga-PSMA-11 by targeted linker design: charged spacer moieties enhance the pharmacokinetic properties. *Bioconjug Chem.* 2017;28:2485–2492.
21. Kratochwil C, Giesel FL, Stefanova M, et al. PSMA-targeted radionuclide therapy of metastatic castration-resistant prostate cancer with ^{177}Lu-labeled PSMA-617. *J Nucl Med.* 2016;57:1170–1176.
22. Hillier SM, Maresca KP, Femia FJ, et al. Preclinical evaluation of novel glutamate-urea-lysine analogues that target prostate-specific membrane antigen as molecular imaging pharmaceuticals for prostate cancer. *Cancer Res.* 2009;69:6932–6940.
23. Chen Y, Foss CA, Byun Y, et al. Radiohalogenated prostate-specific membrane antigen (PSMA)-based ureas as imaging agents for prostate cancer. *J Med Chem.* 2008;51:7933–7943.
24. Wester HJ, Schottelius M, Scheidhauer K, et al. PET imaging of somatostatin receptors: design, synthesis and preclinical evaluation of a novel ^{18}F-labelled, carbohydrated analogue of octreotide. *Eur J Nucl Med Mol Imaging.* 2003;30:117–122.
25. Liu T, Nedrow-Byers JR, Hopkins MR, Berkman CE. Spacer length effects on in vitro imaging and surface accessibility of fluorescent inhibitors of prostate specific membrane antigen. *Bioorg Med Chem Lett.* 2011;21:7013–7016.
26. Benešová M, Bauder-Wust U, Schafer M, et al. Linker modification strategies to control the prostate-specific membrane antigen (PSMA)-targeting and pharmacokinetic properties of DOTA-conjugated PSMA inhibitors. *J Med Chem.* 2016; 59:1761–1775.
27. Grubmüller B, Baum RP, Capasso E, et al. ^{64}Cu-PSMA-617 PET/CT imaging of prostate adenocarcinoma: first in-human studies. *Cancer Biother Radiopharm.* 2016;31:277–286.
28. Cui C, Hanyu M, Hatori A, et al. Synthesis and evaluation of [^{64}Cu]PSMA-617 targeted for prostate-specific membrane antigen in prostate cancer. *Am J Nucl Med Mol Imaging.* 2017;7:40–52.
29. Banerjee SR, Pullambhatla M, Foss CA, et al. ^{64}Cu-labeled inhibitors of prostate-specific membrane antigen for PET imaging of prostate cancer. *J Med Chem.* 2014;57:2657–2669.
30. Gourni E, Canovas C, Goncalves V, Denat F, Meyer PT, Maecke HR. (R)-NODAGA-PSMA: a versatile precursor for radiometal labeling and nuclear imaging of PSMA-positive tumors. *PLoS One.* 2015;10:e0145755.
31. Sevcenco S, Klingler HC, Eredics K, et al. Application of Cu-64 NODAGA-PSMA PET in prostate cancer. *Adv Ther.* 2018;35:779–784.
32. Nedrow JR, Latoche JD, Day KE, et al. Targeting PSMA with a Cu-64 labeled phosphoramidate inhibitor for PET/CT imaging of variant PSMA-expressing xenografts in mouse models of prostate cancer. *Mol Imaging Biol.* 2016;18:402–410.
33. Lewis MR, Wang M, Axworthy DB, et al. In vivo evaluation of pretargeted ^{64}Cu for tumor imaging and therapy. *J Nucl Med.* 2003;44:1284–1292.
34. De Silva RA, Jain S, Lears KA, et al. Copper-64 radiolabeling and biological evaluation of bifunctional chelators for radiopharmaceutical development. *Nucl Med Biol.* 2012;39:1099–1104.
35. Wadas TJ, Wong EH, Weisman GR, Anderson CJ. Copper chelation chemistry and its role in copper radiopharmaceuticals. *Curr Pharm Des.* 2007;13:3–16.
36. Studer M, Kaden TA. One-step synthesis of mono-N-substituted azamacrocycles with a carboxylic group in the side-chain and their complexes with Cu2+ and Ni2+. *Helv Chim Acta.* 1986;69:2081–2086.
37. Boswell CA, Regino CA, Baidoo KE, et al. Synthesis of a cross-bridged cyclam derivative for peptide conjugation and ^{64}Cu radiolabeling. *Bioconjug Chem.* 2008; 19:1476–1484.
38. Schäfer M, Bauder-Wüst U, Leotta K, et al. A dimerized urea-based inhibitor of the prostate-specific membrane antigen for ^{68}Ga-PET imaging of prostate cancer. *EJNMMI Res.* 2012;2:23.
39. Afshar-Oromieh A, Hetzheim H, Kratochwil C, et al. The theranostic PSMA ligand PSMA-617 in the diagnosis of prostate cancer by PET/CT: biodistribution in humans, radiation dosimetry, and first evaluation of tumor lesions. *J Nucl Med.* 2015;56:1697–1705.
40. Zhang AX, Murelli RP, Barinka C, et al. A remote arene-binding site on prostate specific membrane antigen revealed by antibody-recruiting small molecules. *J Am Chem Soc.* 2010;132:12711–12716.
41. Hillier S, Rubino K, Maresca K, et al. [^{131}I] MIP-1466, a small molecule prostate-specific membrane antigen (PSMA) inhibitor for targeted radiotherapy of prostate cancer (PCa) [abstract]. *J Nucl Med.* 2012;53(suppl 1):170.
42. Benešová M, Umbricht CA, Schibli R, Muller C. Albumin-binding PSMA ligands: optimization of the tissue distribution profile. *Mol Pharm.* 2018;15:934–946.
43. Boswell CA, Sun X, Niu W, et al. Comparative in vivo stability of copper-64-labeled cross-bridged and conventional tetraazamacrocyclic complexes. *J Med Chem.* 2004;47:1465–1474.
44. Wong EH, Weisman GR, Hill DC, et al. Synthesis and characterization of cross-bridged cyclams and pendant-armed derivatives and structural studies of their copper(II) complexes. *J Am Chem Soc.* 2000;122:10561–10572.
45. Riesen A, Zehnder M, Kaden TA. Structure of the barium salt of a Cu2+ complex with a tetraaza macrocyclic tetraacetate. *Acta Crystallogr C.* 1988;44:1740–1742.
46. Riesen A, Zehnder M, Kaden TA. Metal complexes of macrocyclic ligands. Part XXIII. Synthesis, properties, and structures of mononuclear complexes with 12- and 14-membered tetraazamacrocycle-N,N′,N″,NΔ-tetraacetic acids. *Helv Chim Acta.* 1986;69:2067–2073.
47. Smith-Jones PM, Fridrich R, Kaden TA, et al. Antibody labeling with copper-67 using the bifunctional macrocycle 4-[(1,4,8,11-tetraazacyclotetradec-1-yl)methyl]benzoic acid. *Bioconjug Chem.* 1991;2:415–421.
48. Eder M, Neels O, Muller M, et al. Novel preclinical and radiopharmaceutical aspects of [^{68}Ga]Ga-PSMA-HBED-CC: a new PET tracer for imaging of prostate cancer. *Pharmaceuticals (Basel).* 2014;7:779–796.
49. Bacich DJ, Pinto JT, Tong WP, Heston WD. Cloning, expression, genomic localization, and enzymatic activities of the mouse homolog of prostate-specific membrane antigen/NAALADase/folate hydrolase. *Mamm Genome.* 2001;12:117–123.
50. Kratochwil C, Giesel FL, Leotta K, et al. PMPA for nephroprotection in PSMA-targeted radionuclide therapy of prostate cancer. *J Nucl Med.* 2015;56:293–298.
51. Rousseau E, Lau J, Kuo HT, et al. Monosodium glutamate reduces ^{68}Ga-PSMA-11 uptake in salivary glands and kidneys in a preclinical prostate cancer model. *J Nucl Med.* 2018;59:1865–1868.
52. Cai H, Wu JS, Muzik O, Hsieh JT, Lee RJ, Peng F. Reduced ^{64}Cu uptake and tumor growth inhibition by knockdown of human copper transporter 1 in xenograft mouse model of prostate cancer. *J Nucl Med.* 2014;55:622–628.
53. Peng F, Lu X, Janisse J, Muzik O, Shields AF. PET of human prostate cancer xenografts in mice with increased uptake of $^{64}CuCl_2$. *J Nucl Med.* 2006;47:1649–1652.
54. Piccardo A, Paparo F, Puntoni M, et al. ^{64}CuCl2 PET/CT in prostate cancer relapse. *J Nucl Med.* 2018;59:444–451.
55. Heroux KJ, Woodin KS, Tranchemontagne DJ, et al. The long and short of it: the influence of N-carboxyethyl versus N-carboxymethyl pendant arms on in vitro and in vivo behavior of copper complexes of cross-bridged tetraamine macrocycles. *Dalton Trans.* 2007;2150–2162.
56. Sun X, Wuest M, Weisman GR, et al. Radiolabeling and in vivo behavior of copper-64-labeled cross-bridged cyclam ligands. *J Med Chem.* 2002;45:469–477.
57. Cole WC, DeNardo SJ, Meares CF, et al. Serum stability of ^{67}Cu chelates: comparison with ^{111}In and ^{57}Co. *Int J Rad Appl Instrum B.* 1986;13:363–368.
58. Meares CF, Moi MK, Diril H, et al. Macrocyclic chelates of radiometals for diagnosis and therapy. *Br J Cancer Suppl.* 1990;10:21–26.
59. Mirick GR, O'Donnell RT, DeNardo SJ, Shen S, Meares CF, DeNardo GL. Transfer of copper from a chelated ^{67}Cu-antibody conjugate to ceruloplasmin in lymphoma patients. *Nucl Med Biol.* 1999;26:841–845.
60. Bass LA, Wang M, Welch MJ, Anderson CJ. In vivo transchelation of copper-64 from TETA-octreotide to superoxide dismutase in rat liver. *Bioconjug Chem.* 2000;11:527–532.
61. Blower PJ, Lewis JS, Zweit J. Copper radionuclides and radiopharmaceuticals in nuclear medicine. *Nucl Med Biol.* 1996;23:957–980.
62. Notni J, Wester H-J. Re-thinking the role of radiometal isotopes: towards a future concept for theranostic radiopharmaceuticals. *J Labelled Comp Radiopharm.* 2018;61:141–153.
63. Yoshii Y, Yoshimoto M, Matsumoto H, et al. Integrated treatment using intraperitoneal radioimmunotherapy and positron emission tomography-guided surgery with ^{64}Cu-labeled cetuximab to treat early- and late-phase peritoneal dissemination in human gastrointestinal cancer xenografts. *Oncotarget.* 2018;9:28935–28950.
64. Su HC, Zhu Y, Hu S-l, et al. The value of ^{99m}Tc-PSMA SPECT/CT-guided surgery for identifying and locating lymph node metastasis in prostate cancer patients. *Ann Surg Oncol.* 2019;26:653–659.